Simulation of Dispersive Multiconductor Transmission Lines by Padé Approximation via the Lanczos Process

Mustafa Celik and Andreas C. Cangellaris, *Member, IEEE*

Abstract—**A mathematical model for dispersive, multiconductor transmission lines is introduced that makes possible the utilization of the Padé approximation via the Lanczos (PVL) process to the analysis of linear networks that contain transmission line systems. The mathematical model is based on the use of Chebyshev polynomials for the representation of the spatial variation of the transmission-line voltages and currents. A simple collocation procedure is used to obtain a matrix representation of the transmission line equations with matrix coefficients that are first order polynomials in the Laplace-transform variable s and in which terminal transmission-line voltages and currents appear explicitly. Thus, the model is compatible with both the PVL algorithm and the modified nodal analysis formalism. Results from the numerical simulation of both digital interconnect-type and microwave circuits are presented to demonstrate the validity and discuss the efficiency of the proposed model.**

I. Introduction

SINCE the introduction of asymptotic waveform evaluation (AWE) [1] in the late 1980's, analysis of large linear circuits using moment-matching techniques has been the subject of extensive research in the CAD area [2]–[11]. The need for such alternative approaches to electronic circuit analysis is mainly driven by the rapid growth in size, density and complexity of modern integrated circuits. For such large circuits, the use of general purpose circuit simulators becomes inefficient or even impossible. The alternative to such simulators is the development of approximate reduced models which capture with acceptable engineering accuracy the important attributes of the response of the circuit over the bandwidth of interest to the specific analysis or design.

Padé moment-matching methods such as AWE and its derivatives, approximate the s-domain transfer function of a linear circuit by a reduced-order model containing only a few number of dominant poles and residues. The time- and frequency-domain responses of the linear circuit can be computed using the reduced-order model. Although moment-matching techniques have been applied with great success to a variety of electrical CAD problems, they are hindered by some numerical limitations.

Recently, a new method was introduced for the computation of the Padé approximation of a lumped linear RLC circuit via the Lanczos process [12]. This algorithm, which is called PVL (Padé via Lanczos), produces more accurate and higher-order approximations compared to AWE and its derivatives. Despite its superior performance to moment-matching techniques, applications of PVL have so far been limited to lumped RLC circuits. The objective of this paper is to introduce a method for modeling circuits with dispersive multiconductor transmission lines using the PVL algorithm.

The organization of this paper is as follows. In Section II, an s-domain relationship is developed for the terminal voltages and currents of multiconductor transmission lines that is consistent with the mathematical formulation used in the PVL method. In Section III, the methodology is extended to transmission lines with frequency-dependent line parameters. The incorporation of this transmission-line model into the modified nodal analysis (MNA) equations of a linear circuit containing sections of multiconductor transmission lines is discussed in Section IV. In Section V, several numerical examples are presented from the application of the proposed model to the PVL analysis of circuits with transmission lines. Comparisons with results from the literature are used to demonstrate the validity of the model. Finally, some concluding remarks are given in Section VI.

II. Transmission Lines

The s-domain Telegrapher's equations for a multiconductor transmission line system of length l are given by

$$\frac{d}{dx'}\boldsymbol{V}(x',s) = -(\boldsymbol{R}(x') + s\boldsymbol{L}(x'))\boldsymbol{I}(x',s) \tag{1}$$

$$\frac{d}{dx'}\boldsymbol{I}(x',s) = -(\boldsymbol{G}(x') + s\boldsymbol{C}(x'))\boldsymbol{V}(x',s) \tag{2}$$

where $\boldsymbol{V}(x')$ and $\boldsymbol{I}(x',s)$ are, respectively, the column vectors of line voltages and currents; $\boldsymbol{R}(x')$, $\boldsymbol{L}(x')$, $\boldsymbol{C}(x')$, and $\boldsymbol{G}(x')$ are, respectively, per-unit-length (p.u.l) resistance, inductance, capacitance, and conductance matrices. For the sake of clarity, the model is first developed for the case of lines with frequency-independent p.u.l. parameters. The extension of the model to lines with frequency-dependent p.u.l. parameters is given in Section III. The general approach to include the multiconductor transmission line systems into a circuit simulator is to treat them as linear multiports described by a suitable relationship between terminal voltages and currents (e.g., Y-parameter representation, h-parameter representation)

Manuscript received March 29, 1996. This work was supported in part by the Semiconductor Research Corporation under Contract 95-PP-086.

The authors are with the Center for Electronic Packaging Research, Department of Electrical and Computer Engineering, University of Arizona, Tucson, AZ 85721 USA.

Publisher Item Identifier S 0018-9480(96)08559-6.

which is obtained rigorously from the integration of Telegrapher's equations. For instance, the following formulation is generally employed to integrate transmission lines into moment-matching type simulations:

$$\boldsymbol{A}(s)\boldsymbol{V}_t(s) + \boldsymbol{B}(s)\boldsymbol{I}_t(s) = 0 \tag{3}$$

where $\boldsymbol{V}_t(s)$ and $\boldsymbol{I}_t(s)$ are column vectors containing, respectively, the terminal voltages and currents of the multiconductor line system. The matrices $\boldsymbol{A}(s)$ and $\boldsymbol{B}(s)$ are described in terms of the per-unit-length line parameters and are usually exponential type functions of s. However, in order to be able to use the PVL technique to analyze circuits containing transmission lines, the elements of the matrices $\boldsymbol{A}(s)$ and $\boldsymbol{B}(s)$ in (3) need to be first-degree polynomials in s. One way to achieve this is to avoid the integration of (1), (2). Instead, a direct numerical approximation of the system of (1) and (2) along the transmission line is sought, that can be effected in such a way that spatial derivatives are calculated explicitly and terminal voltages and currents appear explicitly in the resulting approximation. The development of such an approximation using Chebyshev polynomials for the expansion of $\boldsymbol{V}(x', s)$ and $\boldsymbol{I}(x', s)$ is presented next.

Let l be the length of the transmission line system, i.e., $(0 \leq x' \leq l)$. The transformation $x = 2x'/l - 1$ maps the domain $[0, l]$ onto the domain $[-1, 1]$, which is convenient in dealing with Chebyshev polynomials. For the sake of simplicity, we consider first the simple two-conductor transmission line case; the mathematical model is then generalized for multiconductor transmission line systems.

A. Two-Conductor Transmission Line

The transformed Telegrapher's equations for a two-conductor transmission line of length l, with one of the conductors taken as reference, are:

$$\frac{d}{dx}V(x,s) = -\frac{l}{2}(R(x) + sL(x))I(x,s) \tag{4}$$

$$\frac{d}{dx}I(x,s) = -\frac{l}{2}(G(x) + sC(x))V(x,s). \tag{5}$$

In the proposed methodology, the line voltages and currents are approximated by their truncated Chebyshev expansions:

$$V(x,s) = \sum_{m=0}^{M} a_m(s)T_m(x) \tag{6}$$

$$I(x,s) = \sum_{m=0}^{M} b_m(s)T_m(x) \tag{7}$$

where $T_m(x) = \cos(m\cos^{-1}x)$ is the mth degree Chebyshev polynomial of type 1. The choice of Chebyshev polynomials for the representation of the spatial variation of the transmission line voltage and current is motivated by the exponential rate of convergence of Chebyshev expansions [13]. Because of this property of Chebyshev expansions, highly accurate approximations of the voltage and current distributions along the lines can be effected with a small number of polynomials (M). The choice of M is discussed later.

The use of Chebyshev polynomials for spectral approximations of wave propagation in multiconductor transmission lines has been discussed in [14]. However, for the purposes of our applications, the so-called pseudo-spectral approximation is found to be more convenient [13]. Let $V(x_n, s), I(x_n, s), n = 0, 1, 2, \cdots, M$, be the voltage and current values at the points x_n defined by

$$x_n = \cos\frac{\pi n}{M}, \qquad n = 0, 1, \cdots, M. \tag{8}$$

Clearly, $x_0 = 1$ and $x_M = -1$ correspond, respectively, to the far- and near-end terminals of the transmission line. It can be shown that the coefficients a_m and b_m in (6) and (7) are given by [13]

$$a_m(s) = \frac{2}{M}\frac{1}{c_m}\sum_{n=0}^{M}\frac{V(x_n,s)T_m(x_n)}{c_n} \tag{9}$$

$$b_m(s) = \frac{2}{M}\frac{1}{c_m}\sum_{n=0}^{M}\frac{I(x_n,s)T_m(x_n)}{c_n} \tag{10}$$

where c_m is defined as

$$c_m = \begin{cases} 1, & m \neq 0, M \\ 2, & \text{otherwise.} \end{cases} \tag{11}$$

Substituting (9) and (10) into (6) and (7), respectively, one obtains

$$V(x,s) = \sum_{m=0}^{M} V(x_m,s)g_m(x) \tag{12}$$

$$I(x,s) = \sum_{m=0}^{M} I(x_m,s)g_m(x) \tag{13}$$

where $g_m(x)$ are given by

$$g_m(x) = \frac{(1-x^2)T'_M(x)(-1)^{m+1}}{c_m M^2(x - x_m)}. \tag{14}$$

As expected, the polynomials $g_m(x)$ have the Lagrange polynomial-type property

$$g_m(x_n) = \delta_{mn} \tag{15}$$

where δ_{mn} is the Kronecker delta.

To obtain an approximation to the differential equations given in (4) and (5), a collocation method is used with collocation points those in (8). Substituting (12) and (13) into (4) and (5), one obtains

$$\sum_{m=0}^{M} V(x_m,s)\frac{d}{dx}g_m(x) = -\frac{l}{2}(R(x) + sL(x))\sum_{m=0}^{M} I(x_m,s)g_m(x) \tag{16}$$

$$\sum_{m=0}^{M} I(x_m,s)\frac{d}{dx}g_m(x) = -\frac{l}{2}(G(x) + sC(x))\sum_{m=0}^{M} V(x_m,s)g_m(x). \tag{17}$$

To perform the collocation, the derivatives of polynomials g_m at the collocation points are needed. They are found to be

$$\left.\frac{d}{dx}g_m(x)\right|_{x=x_n} = D_{nm} \tag{18}$$

where

$$D_{nm} = \frac{c_n}{c_m}\frac{(-1)^{n+m}}{x_n - x_m} \qquad (n \neq m) \tag{19}$$

$$D_{nn} = -\frac{x_n}{2(1-x_n^2)}, \quad 1 \leq n \leq M-1,$$

$$D_{00} = \frac{2M^2+1}{6} = -D_{MM}. \tag{20}$$

In view of the above results and definitions, the system of linear equations obtained from the collocation process may be cast in the form

$$\sum_{m=0}^{M} V(x_m,s)D_{nm} = -\frac{l}{2}(R(x_n)+sL(x_n))I_n(s) \tag{21}$$

$$\sum_{m=0}^{M} I(x_m,s)D_{nm} = -\frac{l}{2}(G(x_n)+sC(x_n))V_n(s) \tag{22}$$

for $n = 0, 1, \cdots, M$.

Let $\boldsymbol{D}$ be the $(M+1)\times(M+1)$ square matrix with elements D_{nm}. Then, the above system of equations may be cast in matrix form as follows:

$$\boldsymbol{D}\boldsymbol{V}_s(s) = -\boldsymbol{Z}(s)\boldsymbol{I}_s(s) \tag{23}$$

$$\boldsymbol{D}\boldsymbol{I}_s(s) = -\boldsymbol{Y}(s)\boldsymbol{V}_s(s) \tag{24}$$

where

$$\boldsymbol{V}_s(s) = [V(x_0,s), V(x_1,s), \cdots, V(x_M,s)]^T \tag{25}$$

$$\boldsymbol{I}_s(s) = [I(x_0,s), I(x_1,s), \cdots, I(x_M,s)]^T \tag{26}$$

and $\boldsymbol{Z}(s)$ and $\boldsymbol{Y}(s)$ are diagonal matrices

$$\boldsymbol{Z}(s) = \frac{l}{2}\,\text{diag}\,\{R(x_0)+sL(x_0), R(x_1)+sL(x_1), \cdots, R(x_M)+sL(x_M)\} \tag{27}$$

$$\boldsymbol{Y}(s) = \frac{l}{2}\,\text{diag}\,\{G(x_0)+sC(x_0), G(x_1)+sC(x_1), \cdots, G(x_M)+sC(x_M)\}. \tag{28}$$

The next step is to express (23) and (24) in terms of the terminal voltages and currents of the transmission line. For this purpose, we use the following colon notation to select specific rows and columns of a matrix. Let $\boldsymbol{A}$ be a matrix. Then $\boldsymbol{A}_{(i:j,m:n)}$ is the $(j-i+1)\times(m-n+1)$ submatrix of A that is between the ith and jth rows, and mth and nth columns of $\boldsymbol{A}$. Similarly, $\boldsymbol{A}_{(i:j,m)}$ is a column vector of length $(j-i+1)$ having as elements the elements of the mth column of the matrix $\boldsymbol{A}$ between (and including) rows i and j. Recognizing that (23), (24) constitute the approximation of a two-point boundary value problem, two boundary conditions (involving the values of terminal voltages or the values of the terminal currents or impedance relationships between the terminal voltages and currents) need be specified for the problem to be well posed. This implies that two of the equations in (23), (24) associated with the terminal quantities need be eliminated in favor of the aforementioned boundary conditions. Without loss of generality, the first and last of the equations in (23) are the ones eliminated. Consequently, using the aforementioned colon notation (23) and (24) are cast in the form as shown in (29) at the bottom of the page, where $V_{\text{near}}(s) = V(x_M,s), V_{\text{far}}(s) = V(x_0,s), I_{\text{near}}(s) = I(x_M,s), I_{\text{far}}(s) = -I(x_0,s)$, and

$$\hat{\boldsymbol{V}}_s(s) = [V(x_1,s) \quad V(x_2,s) \quad \cdots \quad V(x_{M-1},s)]^T \tag{30}$$

$$\hat{\boldsymbol{I}}_s(s) = [I(x_1,s) \quad I(x_2,s) \quad \cdots \quad I(x_{M-1},s)]^T. \tag{31}$$

Equation (29) can be written in a more compact form as,

$$(\boldsymbol{A}^R + s\boldsymbol{A}^I)\boldsymbol{V}_t(s) + (\boldsymbol{B}^R + s\boldsymbol{B}^I)\boldsymbol{J}(s) = \boldsymbol{0} \tag{32}$$

where

$$\boldsymbol{J}(s) = \begin{bmatrix} \boldsymbol{I}_t(s) \\ \hat{\boldsymbol{V}}(s) \\ \hat{\boldsymbol{I}}(s) \end{bmatrix} \tag{33}$$

and $\boldsymbol{V}_t = [V_{\text{near}} \; V_{\text{far}}]^T, \boldsymbol{I}_t = [I_{\text{near}} \; I_{\text{far}}]^T$ are, respectively, the vectors of terminal voltages and currents of the line.

B. Multiconductor Transmission Lines

The development of the model for the case of multiconductor transmission lines is similar to the one for the two-conductor line. In this case, the spatial distributions of the voltage and current on each conductor are expanded in Chebyshev series. For an $(N+1)$-conductor line system, with the $(N+1)$st conductor being the reference, the collocation procedure discussed earlier leads to the following system of equations

$$\begin{bmatrix} \boldsymbol{D} & \cdots & \boldsymbol{0} \\ \vdots & \ddots & \vdots \\ \boldsymbol{0} & \cdots & \boldsymbol{D} \end{bmatrix} \begin{bmatrix} \boldsymbol{V}^1(s) \\ \vdots \\ \boldsymbol{V}^N(s) \end{bmatrix} = -\begin{bmatrix} \boldsymbol{Z}^{11}(s) & \cdots & \boldsymbol{Z}^{1N}(s) \\ \vdots & \ddots & \vdots \\ \boldsymbol{Z}^{N1}(s) & \cdots & \boldsymbol{Z}^{NN}(s) \end{bmatrix} \begin{bmatrix} \boldsymbol{I}^1(s) \\ \vdots \\ \boldsymbol{I}^N(s) \end{bmatrix}, \tag{34}$$

$$\begin{bmatrix} \boldsymbol{D}_{(2:M,M+1)} & \boldsymbol{D}_{(2:M,1)} \\ \boldsymbol{Y}_{(1:M+1,M+1)}(s) & \boldsymbol{Y}_{(1:M+1,1)}(s) \end{bmatrix} \begin{bmatrix} V_{\text{near}}(s) \\ V_{\text{far}}(s) \end{bmatrix} + \begin{bmatrix} \boldsymbol{Z}_{(2:M,M+1)}(s) & -\boldsymbol{Z}_{(2:M,1)}(s) & \boldsymbol{Z}_{(2:M,2:M)}(s) & \boldsymbol{D}_{(2:M,2:M)} \\ \boldsymbol{D}_{(1:M+1,M+1)} & -\boldsymbol{D}_{(1:M+1,1)} & \boldsymbol{D}_{(1:M+1,2:M)} & \boldsymbol{Y}_{(1:M+1,2:M)}(s) \end{bmatrix} \begin{bmatrix} I_{\text{near}}(s) \\ I_{\text{far}}(s) \\ \hat{\boldsymbol{I}}_s(s) \\ \hat{\boldsymbol{V}}_s(s) \end{bmatrix} = \begin{bmatrix} \boldsymbol{0} \\ \boldsymbol{0} \end{bmatrix} \tag{29}$$

$$\begin{bmatrix} \boldsymbol{D} & \cdots & \boldsymbol{0} \\ \vdots & \ddots & \vdots \\ \boldsymbol{0} & \cdots & \boldsymbol{D} \end{bmatrix} \begin{bmatrix} \boldsymbol{I}^1(s) \\ \vdots \\ \boldsymbol{I}^N(s) \end{bmatrix} = -\begin{bmatrix} \boldsymbol{Y}^{11}(s) & \cdots & \boldsymbol{Y}^{1N}(s) \\ \vdots & \ddots & \vdots \\ \boldsymbol{Y}^{N1}(s) & \cdots & \boldsymbol{Y}^{NN}(s) \end{bmatrix} \begin{bmatrix} \boldsymbol{V}^1(s) \\ \vdots \\ \boldsymbol{V}^N(s) \end{bmatrix} \quad (35)$$

where $\boldsymbol{V}^i(s)$ is the vector of voltage samples along the ith conductor,

$$\boldsymbol{V}^i(s) = [V^i(x_0, s) \quad V^i(x_1, s) \quad \cdots \quad V^i(x_M, s)] \quad (36)$$

and

$$\boldsymbol{Z}^{ij}(s) = \frac{l}{2} \operatorname{diag}\{R^{ij}(x_0) + sL^{ij}(x_0), R^{ij}(x_1) + sL^{ij}(x_1), \cdots, R^{ij}(x_M) + sL^{ij}(x_M)\} \quad (37)$$

$\boldsymbol{I}^i(s)$ and $\boldsymbol{Y}^{ij}(s)$ are defined similarly. Introducing the vectors of terminal voltages and currents

$$\boldsymbol{V}_{\text{near}}(s) = [V^1(x_M, s), \cdots, V^N(x_M, s)]^T \quad (38)$$

$$\boldsymbol{V}_{\text{far}}(s) = [V^1(x_0, s), \cdots, V^N(x_0, s)]^T \quad (39)$$

$$\boldsymbol{I}_{\text{near}}(s) = [I^1(x_M, s), \cdots, I^N(x_M, s)]^T \quad (40)$$

$$\boldsymbol{I}_{\text{far}}(s) = -[I^1(x_0, s), \cdots, I^N(x_0, s)]^T \quad (41)$$

and rearranging (34) and (35), we obtain (42) as shown at the bottom of the page. In the above equations the following notation has been used. The matrix $\hat{\boldsymbol{D}}_{(i:j,m:n)}$ is an N-block diagonal matrix with each block being the matrix $\boldsymbol{D}_{(i:j,m:n)}$. The matrix $\hat{\boldsymbol{Z}}_{(i:j,m:n)}(s)$ is defined as

$$\hat{\boldsymbol{Z}}_{(i:j,m:n)}(s) = \begin{bmatrix} \boldsymbol{Z}^{11}_{(i:j,m:n)}(s) & \cdots & \boldsymbol{Z}^{1N}_{(i:j,m:n)}(s) \\ \vdots & \ddots & \vdots \\ \boldsymbol{Z}^{N1}_{(i:j,m:n)}(s) & \cdots & \boldsymbol{Z}^{NN}_{(i:j,m:n)}(s) \end{bmatrix} \quad (43)$$

$\hat{\boldsymbol{V}}(s) = [\hat{\boldsymbol{V}}^1(s), \cdots, \hat{\boldsymbol{V}}^N(s)]$, where $\hat{\boldsymbol{V}}^i(s)$ is given in (30). Finally, $\hat{\boldsymbol{Y}}_{(i:j,m:n)}(s)$ and $\hat{\boldsymbol{I}}(s)$ are defined similarly to $\hat{\boldsymbol{Z}}_{(i:j,m:n)}(s)$ and $\hat{\boldsymbol{V}}(s)$.

Equation (42) can be written in compact form as

$$(\boldsymbol{A}^R + s\boldsymbol{A}^I)\boldsymbol{V}_t(s) + (\boldsymbol{B}^R + s\boldsymbol{B}^I)\boldsymbol{J}(s) = \boldsymbol{0} \quad (44)$$

where

$$\boldsymbol{J}(s) = \begin{bmatrix} \boldsymbol{I}_t(s) \\ \hat{\boldsymbol{V}}(s) \\ \hat{\boldsymbol{I}}(s) \end{bmatrix} \quad (45)$$

and $\boldsymbol{V}_t = [\boldsymbol{V}^T_{\text{near}} \; \boldsymbol{V}^T_{\text{far}}]^T$, $\boldsymbol{I}_t = [\boldsymbol{I}^T_{\text{near}} \; \boldsymbol{I}^T_{\text{far}}]^T$ are the vectors of terminal voltages and currents of the line system, respectively.

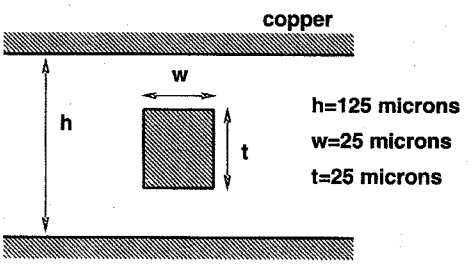

The stripline structure

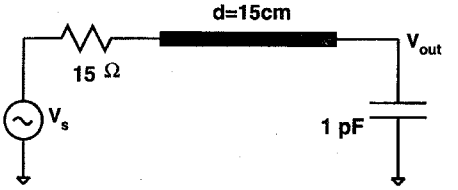

The stripline circuit

Fig. 1. The circuit for example 1.

C. Order of Chebyshev Approximation

One may eliminate the vectors $\hat{\boldsymbol{V}}(s)$ and $\hat{\boldsymbol{I}}(s)$ in (44) and obtain a relation in terms of terminal voltages and currents only. However, in order to be able to use the PVL algorithm for the analysis of transmission lines, the coefficient matrices in (44) must be first degree polynomials in s. This is why we enter (44) as a stamp into the overall circuit matrix. Because of this, it is important to keep the order of Chebyshev approximation as small as possible so that the size of the overall circuit matrix does not become prohibitively large. The accuracy of the approximation, on the other hand, depends on the order, M, of the Chebyshev approximation. To find an optimum value for M we use the result

$$\sin(N\pi x) = 2\sum_{m=0}^{\infty} \frac{1}{c_m} J_m(N\pi) \sin\left(\frac{m\pi}{2}\right) T_m(x), \quad -1 \le x \le 1 \quad (46)$$

where $J_m(z)$ is the Bessel function of order m. Since $J_m(z) \sim (1/\sqrt{2\pi m})(ez/m)^m$ as $m \to \infty$, it is clear that $J_m(N\pi) \to 0$ exponentially fast as $m > N\pi$. This result indicates that the Chebyshev approximation will start converge rapidly when the number of polynomials retained per wavelength is greater than π. Consequently, a heuristic rule for the resolution requirements of Chebyshev expansions is at least four collocation points per wavelength. Therefore, for a transmission

$$\begin{bmatrix} \hat{\boldsymbol{D}}_{(2:M,M+1)} & \hat{\boldsymbol{D}}_{(2:M,1)} \\ \hat{\boldsymbol{Y}}_{(1:M+1,M+1)}(s) & \hat{\boldsymbol{Y}}_{(1:M+1,1)}(s) \end{bmatrix} \begin{bmatrix} \boldsymbol{V}_{\text{near}}(s) \\ \boldsymbol{V}_{\text{far}}(s) \end{bmatrix} + \begin{bmatrix} \hat{\boldsymbol{Z}}_{(2:M,M+1)}(s) & -\hat{\boldsymbol{Z}}_{(2:M,1)}(s) & \hat{\boldsymbol{Z}}_{(2:M,2:M)}(s) & \hat{\boldsymbol{D}}_{(2:M,2:M)} \\ \hat{\boldsymbol{D}}_{(1:M+1,M+1)} & -\hat{\boldsymbol{D}}_{(1:M+1,1)} & \hat{\boldsymbol{D}}_{(1:M+1,2:M)} & \hat{\boldsymbol{Y}}_{(1:M+1,2:M)}(s) \end{bmatrix} \begin{bmatrix} \boldsymbol{I}_{\text{near}}(s) \\ \boldsymbol{I}_{\text{far}}(s) \\ \hat{\boldsymbol{I}}(s) \\ \hat{\boldsymbol{V}}(s) \end{bmatrix} = \begin{bmatrix} \boldsymbol{0} \\ \boldsymbol{0} \end{bmatrix} \quad (42)$$

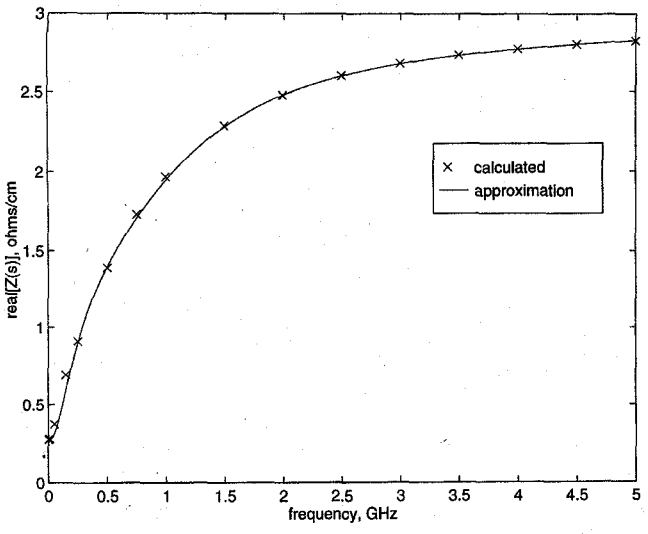

Fig. 2. Comparison of approximated and calculated values of $\mathrm{Re}[Z(j\omega)]$.

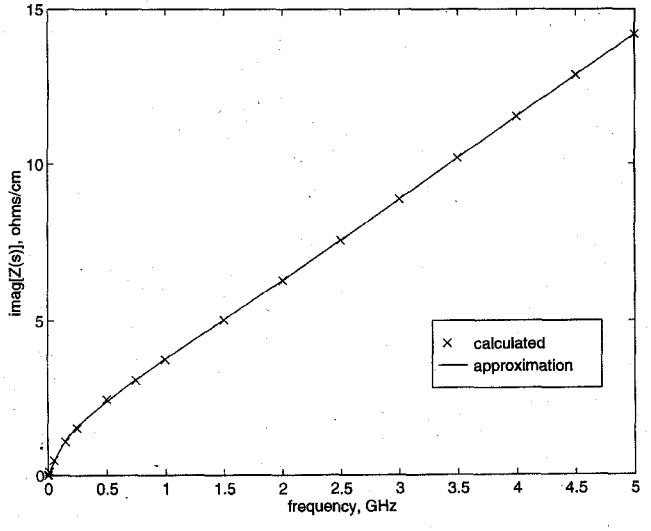

Fig. 3. Comparison of approximated and calculated values of $\mathrm{Im}[Z(j\omega)]$.

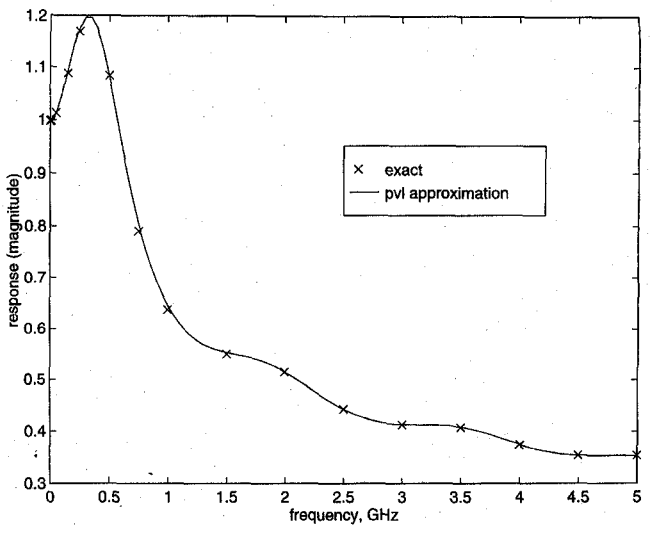

Fig. 4. The output frequency response of the circuit of Example 1.

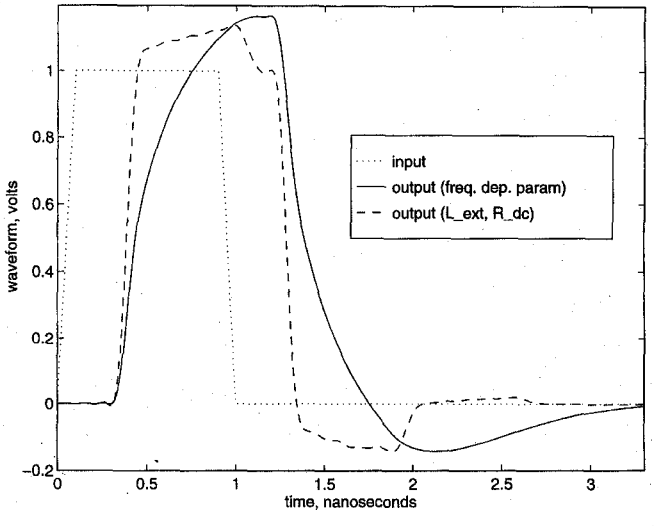

Fig. 5. The transient response of the circuit of Example 1.

line of length l, with $\lambda_{\min}$ the minimum wavelength at the predetermined maximum frequency, $f_{\max}$, the order of approximation, M, is chosen as

$$M = 4\frac{l}{\lambda_{\min}} + 2. \tag{47}$$

III. Transmission Lines with Frequency-Dependent Line Parameters

It is well-known that high-frequency wave propagation in transmission lines in inhomogeneous media is characterized by geometric dispersion. Furthermore, lossy substrates and the finite conductivity of the conductors combine with the aforementioned geometric dispersion and result in equivalent p.u.l. capacitance, inductance, conductance, and resistance matrices that are frequency dependent. This frequency dependence of the line parameters needs to be taken into account for the accurate simulation of high-speed pulse propagation in interconnects or the design of distributed passives for microwave and millimeter-wave applications. In the following, we extend the methodology of the previous section to the case of multiconductor transmission lines with frequency-dependent line parameters. The development begins with the simple case of a two-conductor line and it is subsequently generalized for the case of a multiconductor system.

Even though the proposed methodology is also applicable to nonuniform transmission lines, we choose to develop the model for the case of a uniform line in order to keep the notation as simple as possible. For a uniform transmission line with frequency-dependent line parameters the transformed Telegrapher's equations given in (4) and (5) become

$$\frac{d}{dx}V(x,s) = -\frac{l}{2}Z(s)I(x,s) \tag{48}$$

$$\frac{d}{dx}I(x,s) = -\frac{l}{2}Y(s)V(x,s) \tag{49}$$

where $Z(s)$ and $Y(s)$ are the per-unit-length impedance and admittance functions, respectively. The p.u.l. impedance and admittance functions are related to the p.u.l. line parameters

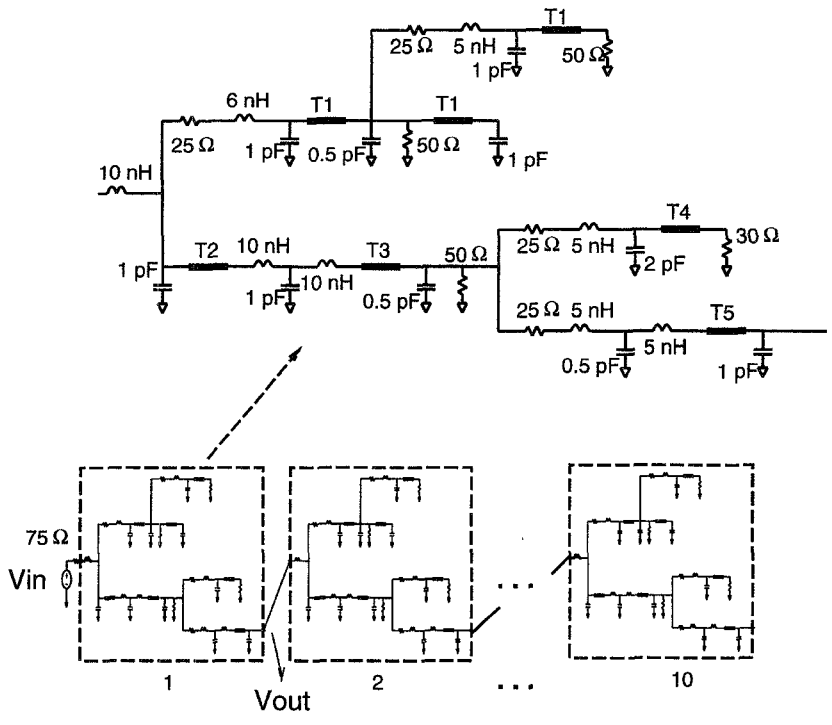

Fig. 6. The circuit for Example 2.

(R, L, C, and G) through the expressions

$$Z(s=j\omega)=R(\omega)+j\omega L(\omega) \tag{50}$$

$$Y(s=j\omega)=G(\omega)+j\omega C(\omega). \tag{51}$$

It will be assumed that the p.u.l. line parameters are either calculated over the frequency range of interest using a suitable full-wave electromagnetic analysis method, or are determined from measurements. In the proposed method, we approximate the p.u.l. impedance and admittance functions with rational functions of s

$$Z(s)=\frac{b_Z(s)}{a_Z(s)}=\frac{b_{Z0}+\cdots+b_{Zq}s^q}{a_{Z0}+\cdots+a_{Zq}s^q} \tag{52}$$

$$Y(s)=\frac{b_Y(s)}{a_Y(s)}=\frac{b_{Y0}+\cdots+b_{Yq}s^q}{a_{Y0}+\cdots+a_{Yq}s^q} \tag{53}$$

where q is the maximum of the orders of the four polynomials. The coefficients of the rational functions are forced to be real and obtained from the available R, L, C, G data using least squares fitting.

Then the MNA stamp given in (29) becomes (54) as shown at the bottom of the page, where 1's and 0's are identity matrices and column vectors of zeros, respectively, with suitable sizes. Multiplying the first $M-1$ rows of the above matrices with $a_Z(s)$ and the remaining $M+1$ rows with $a_Y(s)$, we obtain

$$(\boldsymbol{A}_0+\boldsymbol{A}_1 s+\cdots \boldsymbol{A}_q s^q)\boldsymbol{V}_t+(\boldsymbol{B}_0+\boldsymbol{B}_1 s+\cdots \boldsymbol{B}_q s^q)\boldsymbol{J}=\boldsymbol{0} \tag{55}$$

where

$$\boldsymbol{A}_i=\left[\begin{array}{c|c} a_{Zi}\cdot \boldsymbol{D}_{(2:M,M+1)} & a_{Zi}\cdot \boldsymbol{D}_{(2:M,1)} \\ \hline \boldsymbol{0} & b_{Yi} \\ b_{Yi} & \boldsymbol{0} \end{array}\right] \tag{56}$$

and while the expression for B_i is given by (57) at the bottom of the next page.

$$\left[\begin{array}{c|c} \boldsymbol{D}_{(2:M,M+1)} & \boldsymbol{D}_{(2:M,1)} \\ \hline \boldsymbol{0} & \dfrac{b_Y(s)}{a_Y(s)} \\ \dfrac{b_Y(s)}{a_Y(s)} & \boldsymbol{0} \end{array}\right]\left[\begin{array}{c} V_{\text{near}}(s) \\ V_{\text{far}}(s) \end{array}\right]$$

$$+\left[\begin{array}{c|c|c|c} \boldsymbol{0} & \boldsymbol{0} & \dfrac{b_Z(s)}{a_Z(s)}\boldsymbol{1} & \boldsymbol{D}_{(2.M,2:M)} \\ \hline \boldsymbol{D}_{(1:M+1,M+1)} & -\boldsymbol{D}_{(1:M+1,1)} & \boldsymbol{D}_{(1:M+1,2:M)} & \begin{array}{c} \boldsymbol{0}^T \\ \dfrac{b_Y(s)}{a_Y(s)}\boldsymbol{1} \\ \boldsymbol{0}^T \end{array} \end{array}\right]\left[\begin{array}{c} I_{\text{near}}(s) \\ I_{\text{far}}(s) \\ \hat{\boldsymbol{I}}_s(s) \\ \hat{\boldsymbol{V}}_s(s) \end{array}\right]=\left[\begin{array}{c} \boldsymbol{0} \\ \boldsymbol{0} \end{array}\right] \tag{54}$$

Next, we introduce a set of new vectors

$$\begin{aligned} s\boldsymbol{V}_t &= \boldsymbol{V}_{t2} \\ s\boldsymbol{V}_{t2} &= \boldsymbol{V}_{t3} \\ &\vdots \\ s\boldsymbol{V}_{t(q-1)} &= \boldsymbol{V}_{tq} \end{aligned} \tag{58}$$

and

$$\begin{aligned} s\boldsymbol{J} &= \boldsymbol{J}_2 \\ s\boldsymbol{J}_2 &= \boldsymbol{J}_3 \\ &\vdots \\ s\boldsymbol{J}_{q-1} &= \boldsymbol{J}_q. \end{aligned} \tag{59}$$

Then (55), using (58) and (59), may be cast in the form shown at the bottom of the page preceding (57), where 0's are either column vectors or matrices of zeros with suitable sizes. A compact form of the equation is

$$(\boldsymbol{A}^R + s\boldsymbol{A}^I)\boldsymbol{V}_t(s) + (\boldsymbol{B}^R + s\boldsymbol{B}^I)\boldsymbol{J}^{\text{fdc}}(s) = \boldsymbol{0} \tag{60}$$

where the superscript "fdc" is used to indicate the frequency-dependent case. If the line has frequency-independent parameters, (32) is stamped into the MNA matrix instead of (60).

This result for the two-conductor line can be extended easily to the case of multiconductor transmission line systems. For such systems, the entries of the p.u.l. impedance and admittance matrices are approximated as

$$Z^{ij} = \frac{b_Z^{ij}(s)}{a_Z^i(s)}, \qquad i,j = 1,\cdots,N \tag{61}$$

$$Y^{ij} = \frac{b_Y^{ij}(s)}{a_Y^i(s)}, \qquad i,j = 1,\cdots,N. \tag{62}$$

The reason for choosing the same denominator polynomial for all entries in a row of the p.u.l. impedance and admittance matrices can be explained as follows. In the MNA stamp of a multiconductor transmission line system, any row contains only one row of either the p.u.l. impedance or admittance matrix. Therefore, when we multiply that row with $a_Z^i(s)$ or $a_Y^i(s)$, we obtain an equation set which has polynomials in s as coefficients and the maximum order of these polynomials is kept as small as possible.

IV. Circuit Formulation

Consider a linear circuit $\mathcal{N}$ which contains linear lumped components and multiconductor transmission line systems. Without loss of generality, the time-domain MNA matrix equations for the circuit $\mathcal{N}$ with an impulse excitation as input can be written as [15]

$$\boldsymbol{C}_{\mathcal{N}}\frac{d\boldsymbol{v}_{\mathcal{N}}(t)}{dt} + \boldsymbol{G}_{\mathcal{N}}\boldsymbol{v}_{\mathcal{N}}(t) + \sum_{k=1}^{K}\boldsymbol{P}_k\boldsymbol{i}_k(t) = \boldsymbol{b}_{\mathcal{N}}\delta(t) \tag{63}$$

where $\boldsymbol{v}_{\mathcal{N}}(t)$ is a vector of size $N_{\mathcal{N}}$ containing the waveforms of the node voltages, independent voltage source currents, and inductor currents; $\boldsymbol{b}_{\mathcal{N}}\delta(t)$ is a vector representing the excitations from the independent source; $\boldsymbol{G}_{\mathcal{N}}$ and $\boldsymbol{C}_{\mathcal{N}}$ are constant matrices formed by linear lumped components; $\boldsymbol{P}_k$ is a $N_{\mathcal{N}} \times 2n_k$ selector matrix, whose entries are one or zero, that maps $\boldsymbol{i}_k(t)$, the terminal currents of the kth line system, into the node space of the circuit $\mathcal{N}$; K is the number of transmission-line systems and n_k is the number of conductors in the kth transmission-line system.

The transmission lines are described in the frequency domain by (44). For example, for the kth transmission line system we have

$$(\boldsymbol{A}_k^R + s\boldsymbol{A}_k^I)\boldsymbol{V}_k(s) + (\boldsymbol{B}_k^R + s\boldsymbol{B}_k^I)\boldsymbol{J}_k(s) = \boldsymbol{0} \tag{64}$$

where

$$\boldsymbol{J}_k(s) = \begin{bmatrix} \boldsymbol{I}_k(s) \\ \hat{\boldsymbol{I}}_k(s) \\ \hat{\boldsymbol{V}}_k(s) \end{bmatrix}. \tag{65}$$

(For the case of dispersive transmission line systems we use the multiconductor equivalent of (60). In this case the blocks shown as $[\boldsymbol{P}_i\ 0\ 0]$ in (66) are replaced with $[\boldsymbol{P}_i\ 0\ \cdots\ 0]$ with suitable number of zero matrices.) Combining the formulations

$$\begin{bmatrix} \boldsymbol{A}_0 + s\boldsymbol{A}_1 \\ \boldsymbol{0} \\ \boldsymbol{0} \\ \vdots \\ \boldsymbol{0} \\ s\boldsymbol{1} \\ \boldsymbol{0} \\ \vdots \\ \boldsymbol{0} \end{bmatrix} \boldsymbol{V}_t + \begin{bmatrix} \boldsymbol{B}_0 + s\boldsymbol{B}_1 & s\boldsymbol{B}_2 & s\boldsymbol{B}_3 & \cdots & s\boldsymbol{B}_q & s\boldsymbol{A}_2 & s\boldsymbol{A}_3 & \cdots & s\boldsymbol{A}_q \\ s\boldsymbol{1} & -\boldsymbol{1} & \boldsymbol{0} & \cdots & \boldsymbol{0} & \boldsymbol{0} & \boldsymbol{0} & \cdots & \boldsymbol{0} \\ \boldsymbol{0} & s\boldsymbol{1} & -\boldsymbol{1} & \cdots & \boldsymbol{0} & \boldsymbol{0} & \boldsymbol{0} & \cdots & \boldsymbol{0} \\ \vdots & \vdots & \vdots & \vdots & \vdots & \vdots & \vdots & \vdots & \vdots \\ \boldsymbol{0} & \boldsymbol{0} & \boldsymbol{0} & \cdots & -\boldsymbol{1} & \boldsymbol{0} & \boldsymbol{0} & \cdots & \boldsymbol{0} \\ \boldsymbol{0} & \boldsymbol{0} & \boldsymbol{0} & \cdots & \boldsymbol{0} & -\boldsymbol{1} & \boldsymbol{0} & \cdots & \boldsymbol{0} \\ \boldsymbol{0} & \boldsymbol{0} & \boldsymbol{0} & \cdots & \boldsymbol{0} & s\boldsymbol{1} & -\boldsymbol{1} & \cdots & \boldsymbol{0} \\ \vdots & \vdots & \vdots & \vdots & \vdots & \vdots & \vdots & \vdots & \vdots \\ \boldsymbol{0} & \boldsymbol{0} & \boldsymbol{0} & \cdots & \boldsymbol{0} & \boldsymbol{0} & \boldsymbol{0} & \cdots & -\boldsymbol{1} \end{bmatrix} \begin{bmatrix} \boldsymbol{J} \\ \boldsymbol{J}_2 \\ \boldsymbol{J}_3 \\ \vdots \\ \boldsymbol{J}_q \\ \boldsymbol{V}_{t2} \\ \boldsymbol{V}_{t3} \\ \vdots \\ \boldsymbol{V}_{tq} \end{bmatrix} = \begin{bmatrix} \boldsymbol{0} \\ \boldsymbol{0} \\ \boldsymbol{0} \\ \vdots \\ \boldsymbol{0} \\ \boldsymbol{0} \\ \boldsymbol{0} \\ \vdots \\ \boldsymbol{0} \end{bmatrix}$$

$$\boldsymbol{B}_i = \left[\begin{array}{c|c|c|c} \boldsymbol{0} & \boldsymbol{0} & b_{Zi}\cdot\boldsymbol{1} & a_{Zi}\cdot\boldsymbol{D}_{(2:M,2:M)} \\ \hline a_{Yi}\cdot\boldsymbol{D}_{(1:M+1,M+1)} & -a_{Yi}\cdot\boldsymbol{D}_{(1:M+1,1)} & a_{Yi}\cdot\boldsymbol{D}_{(1:M+1,2:M)} & \begin{matrix}\boldsymbol{0}^T \\ b_{Yi}\cdot\boldsymbol{1} \\ \boldsymbol{0}^T\end{matrix} \end{array}\right] \tag{57}$$

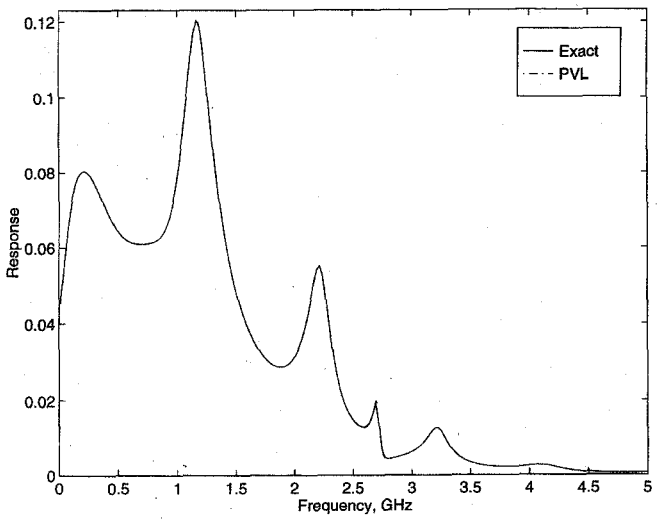

Fig. 7. The output frequency response of the circuit of Example 2.

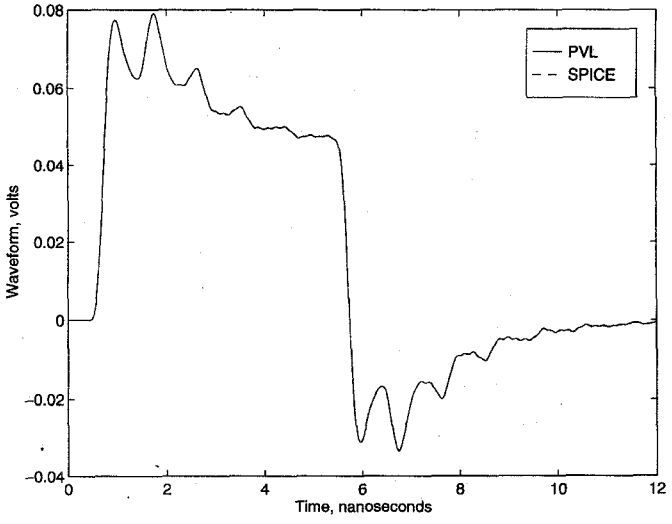

Fig. 8. The transient response of the circuit of Example 2.

for all transmission lines with the Laplace transform of (63), one obtains the frequency-domain MNA matrix for the circuit $\mathcal{N}$ as shown in (66) at the bottom of the page, which may also be written in the familiar compact form

$$(\overline{\boldsymbol{G}} + s\overline{\boldsymbol{C}})\boldsymbol{X} = \boldsymbol{b} \tag{67}$$

Let $H(s)$ be the output of interest

$$H(s) = \boldsymbol{d}^T \boldsymbol{X}(s). \tag{68}$$

Then, using (67), the output frequency response is given by

$$H(s) = \boldsymbol{d}^T (\overline{\boldsymbol{G}} + s\overline{\boldsymbol{C}})^{-1} \boldsymbol{b}. \tag{69}$$

The aim of the PVL algorithm is to find the Padé approximation of the frequency response via Lanczos process

$$H_q = \sum_{i=1}^{q} \frac{k_i}{s - p_i} \tag{70}$$

where q is the order of approximation, and p_i and k_i are, respectively, the poles and the corresponding residues. For the sake of completeness we give a summary of the PVL algorithm in the Appendix.

The PVL algorithm can also be used to find reduced-order macromodels for large linear blocks [16]. The linear blocks are replaced by their reduced order models, and then the equivalent smaller circuit can be analyzed using a standard numerical integration simulator such as SPICE.

We conclude this section by a short discussion of the issue of positive poles produced by the PVL algorithm. As discussed in detail in [16], even if the linear system itself is stable, the PVL algorithm may produce some poles with positive real parts in the early stages of the iteration. This was the case for several of the circuits we examined. However, the positive poles that occured were either far from the frequency range of interest or their residues were negligible. These results agree with those in [16]. Thus for the purpose of reduced-order modeling of a circuit using the poles and residues produced by the PVL algorithm, any positive poles (that occured after the Padé approximation had converged over the frequency range of interest) were not included in the final pole/residue representation.

V. Numerical Experiments

We have implemented a PVL simulator using SPICE3f4 [17]. This enhanced version of SPICE3f4 can simulate complicated circuits with multiple transmission lines with both spatially varying and frequency-dependent p.u.l. parameters. In addition, the PVL algorithm can be used to generate reduced-order models for these distributed circuits. The following examples are used to demonstrate some of the features of this simulator.

Example 1: The stripline structure shown in Fig. 1 was analyzed using the method given in [18] and the p.u.l. line inductance and resistance parameters were calculated at a set of frequency points. Since the dielectric is homogeneous and lossless, only the p.u.l. inductance and resistance of the line is frequency dependent. The purpose of this simple example was to test the validity of the proposed implementation of disper-

$$\begin{bmatrix} \boldsymbol{G}_{\mathcal{N}} + s\boldsymbol{C}_{\mathcal{N}} & [\boldsymbol{P}_1\ \mathbf{0}\ \mathbf{0}] & [\boldsymbol{P}_2\ \mathbf{0}\ \mathbf{0}] & \cdots & [\boldsymbol{P}_K\ \mathbf{0}\ \mathbf{0}] \\ (\boldsymbol{A}_1^R + s\boldsymbol{A}_1^I)\boldsymbol{P}_1^T & \boldsymbol{B}_1^R + s\boldsymbol{B}_1^I & \mathbf{0} & \cdots & \mathbf{0} \\ (\boldsymbol{A}_2^R + s\boldsymbol{A}_2^I)\boldsymbol{P}_2^T & \mathbf{0} & \boldsymbol{B}_2^R + s\boldsymbol{B}_2^I & \cdots & \mathbf{0} \\ \vdots & \vdots & \vdots & & \vdots \\ (\boldsymbol{A}_K^R + s\boldsymbol{A}_K^I)\boldsymbol{P}_K^T & \mathbf{0} & \mathbf{0} & \cdots & \boldsymbol{B}_K^R + s\boldsymbol{B}_K^I \end{bmatrix} \begin{bmatrix} \boldsymbol{V}_{\mathcal{N}}(s) \\ \boldsymbol{J}_1(s) \\ \boldsymbol{J}_2(s) \\ \vdots \\ \boldsymbol{J}_K(s) \end{bmatrix} = \begin{bmatrix} \boldsymbol{b}_{\mathcal{N}} \\ \mathbf{0} \\ \mathbf{0} \\ \vdots \\ \mathbf{0} \end{bmatrix} \tag{66}$$

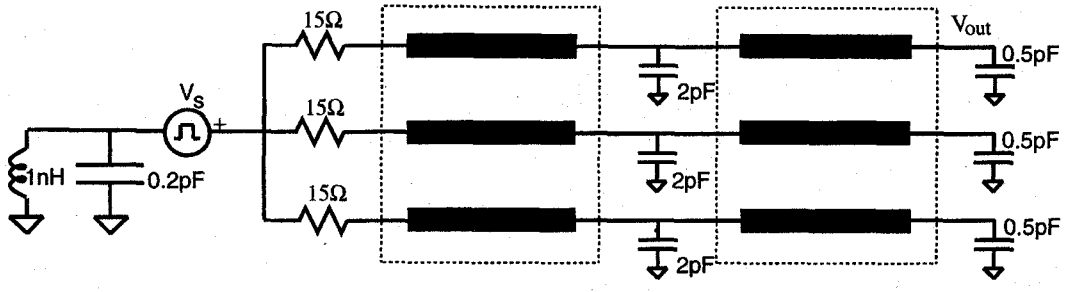

Fig. 9. The circuit for Example 3.

sive interconnects in SPICE3f4 using Chebyshev expansions, as well as test the implementation of the PVL algorithm.

A third-order rational function approximation for the impedance function, $Z(s)$, was obtained using MATLAB's INVFREQS routine [19]. As illustrated in Figs. 2 and 3, the agreement of the calculated values (R and ωL) with the values obtained from these rational function approximations ($\mathrm{Re}[Z(j\omega)]$ and $\mathrm{Im}[Z(j\omega)]$), is excellent. The other p.u.l. line parameters are $C = 1$ pF/cm and $G = 0$. Taking the maximum frequency of interest as 5 GHz, the order of the Chebyshev expansion, M, was chosen as 9 according to (47). The proposed methodology was then used to obtain the 25th order PVL approximation for the voltage response at the output node. Fig. 4 depicts the comparison of the magnitude of the calculated response with exact results obtained (using standard frequency-domain transmission line analysis) at the frequency points at which the line parameters were calculated. The agreement is excellent. Next, the transient response at the output node was calculated for a 1 V input pulse of 0.1 ns rise and fall times and 1 ns duration. Fig. 5 depicts the comparison of the output voltage obtained using the frequency-dependent R and L parameters with that obtained using frequency-independent values for R and L, namely, the (infinite-frequency) external inductance value for L and the dc value for R. Clearly, the pulse suffers significant dispersion which is not accurately modeled using simply the dc value of the p.u.l. resistance.

Example 2: The next example deals with the interconnection circuit shown in Fig. 6. The circuit shown at the top of the figure was repeated ten times as shown at the bottom part of the figure. The resulting circuit has a total of 70 transmission lines. There are five different transmission lines. All lines are assumed to have negligible p.u.l. conductance while their p.u.l. resistance is taken to be 0.1 ohms/cm. The remaining p.u.l. parameters, C and, L, and the length l of the lines are: Line T1, $C = 1$ pF/cm, $L = 0.6$ nH/cm, $l = 3$ cm. Line T2, $C = 1$ pF/cm, $L = 1$ nH/cm, $l = 5$ cm. Line T3, $C = 1.2$ pF/cm, $L = 0.6$ nH/cm, $l = 3$ cm. Line T4, $C = 1$ pF/cm, $L = 0.6$ nH/cm, $l = 4$ cm. Line T5, $C = 1.5$ pF/cm, $L = 1$ nH/cm, $l = 2$ cm.

A PVL approximation of order 40 was generated for the response at the node indicated as V_{out} in the figure. The comparison of the frequency response provided by the PVL approximation with that generated using standard SPICE is depicted in Fig. 7. The two responses are indistinguishable. The time-domain response at the same node, for a 1 V input pulse of 100 ps rise/fall time and 5 ns duration, was also

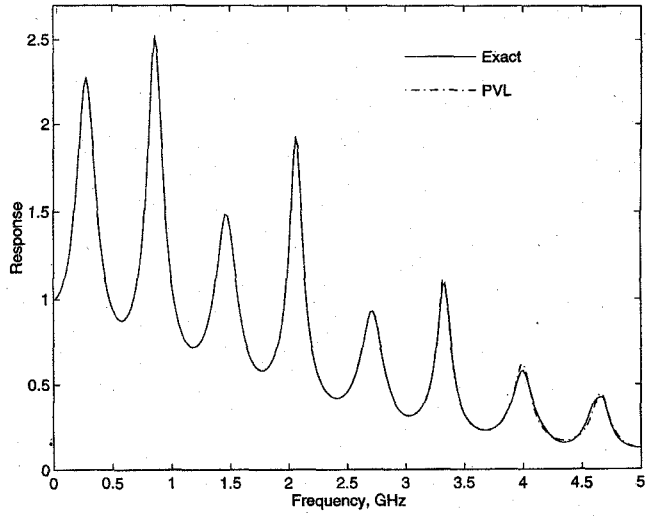

Fig. 10. The output frequency response of the circuit of Example 3.

computed. It is compared with the SPICE3f4 result in Fig. 8. The agreement is excellent.

The CPU time needed for the generation of the 40th order PVL approximation was 1.83 seconds on a SUN Sparc10. This runtime does not include the eigendecomposition of the matrix $\boldsymbol{T}_q$ which requires 0.48 seconds in MATLAB [19] on a DEC 5000. The distribution of the CPU time consumption is given in Table I. This time should be compared with the time of 835.5 seconds required by the regular version of SPICE3f4 running on the same SUN Sparc10 platform to generate the waveform of Fig. 8.

Example 3: This examples deals with the packaging interconnection system shown in Fig. 9. The coupled lines are identical and their length is $l = 5$ cm. The per-unit-length line parameters are

$$\boldsymbol{R} = \begin{bmatrix} 3.448 & 0 & 0 \\ 0 & 3.448 & 0 \\ 0 & 0 & 3.448 \end{bmatrix} \ \Omega/\text{cm} \tag{71}$$

$$\boldsymbol{L} = \begin{bmatrix} 4.976 & 0.765 & 0.152 \\ 0.765 & 4.976 & 0.765 \\ 0.152 & 0.765 & 4.976 \end{bmatrix} \ \text{nH/cm} \tag{72}$$

$$\boldsymbol{C} = \begin{bmatrix} 1.082 & -0.197 & -0.006 \\ -0.197 & 1.124 & -0.197 \\ -0.006 & -0.197 & 1.082 \end{bmatrix} \ \text{pF/cm}. \tag{73}$$

Dielectric losses are assumed negligible. The frequency response for V_{out} is shown in Fig. 10. The order of the PVL aprroximation is 40. This circuit was also analyzed using

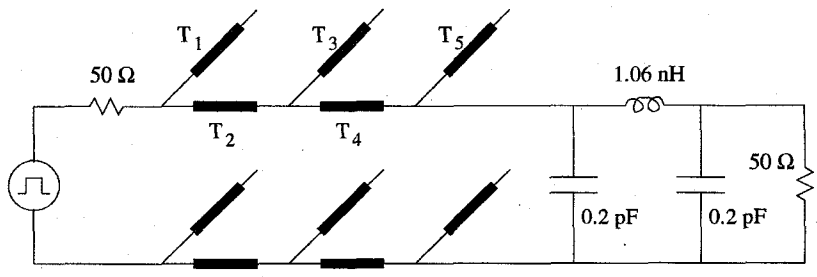

Fig. 11. The circuit for Example 4.

TABLE I
THE CPU TIME ANALYSIS ON A SUN Sparc10 FOR EXAMPLE 2

Operation	CPU time in seconds
Reordering and LU decomposition	0.40
Forward and back substitutions	0.59
Other operations	0.54
Total Lanczos time	1.53
Input/output	0.30
Total time	1.83

multipoint Padé approximation with 5 expansion points [11]. However, the expansion points are selected in a heuristic manner in the multipoint Padé approximation. Alternatively, complex frequency hopping (CFH) [8] could have been used to take advantage of its automated procedure for the selection of the expansion points. However, the required number of hops, which is usually twice the number of expansion points needed for multipoint Padé approximation for same accuracy, would be rather large.

Example 4: The final example considers a low-pass filter implemented with transmission lines as as shown in Fig. 11. The filter has a cut-off frequency of 4 GHz. All transmission-line sections are assumed lossless and are of length $\lambda/8$ at the cut-off frequency. Their per-unit-length parameters are: $L_1 = L_5 = 2.1633$ nH/cm, $C_1 = C_5 = 0.5136$ pF/cm; $L_2 = L_4 = 7.25$ nH/cm, $C_2 = C_4 = 0.153\,26$ pF/cm; $L_3 = 2.3433$ nH/cm, $C_3 = 0.474\,16$ pF/cm. This filter was successfully analyzed in [9] using multipoint Padé approximation technique with expansion points at 0, 12.5, 25, 37.5, and 50 GHz. The response obtained after 70 PVL iterations is compared with the exact response in Fig 12. The agreement over the 0 GHz–50 GHz band is excellent.

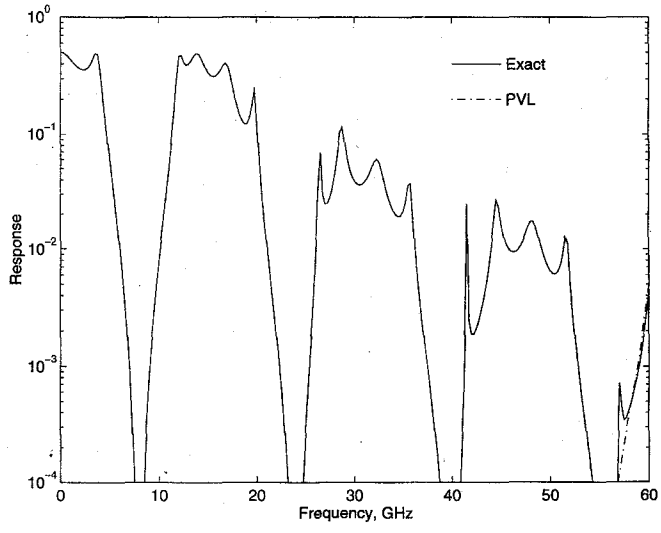

Fig. 12. The output frequency response of the circuit of Example 4.

VI. CONCLUSION

In conclusion, we have introduced a mathematical model that allows linear circuits with dispersive, multiconductor transmission lines to be simulated by the PVL algorithm. The mathematical model is based on the use of Chebyshev expansions for the representation of the spatial variation of the transmission-line voltages and currents. Through a simple collocation procedure, an s-domain matrix representation of the multiconductor transmission line system is derived. The coefficient matrices in this representation are first-degree polynomials in s. Furthermore, the terminal voltages and currents appear explicitly in this representation. Consequently, the representation is compatible with the PVL algorithm, and its integration into the MNA matrix for the circuit containing the transmission lines is straightforward.

The exponential rate of convergence of Chebyshev polynomial expansions leads to highly accurate approximations of the the voltage/current spatial variation on the lines using only four polynomials per wavelength. Keeping the number of terms in the transmission-line voltage/current expansions small is very important since it controls the size of the resulting MNA matrix.

Several circuits were analyzed using a computer implementation of the proposed methodology. Both digital interconnect-type circuits and microwave circuits were modeled with excellent accuracy over very broad frequency ranges.

APPENDIX
THE PVL ALGORITHM

First we define

$$\boldsymbol{A} = -(\overline{\boldsymbol{G}} + s_0\overline{\boldsymbol{C}})^{-1}\overline{\boldsymbol{C}}, \quad \boldsymbol{r} = (\overline{\boldsymbol{G}} + s_0\overline{\boldsymbol{C}})^{-1}\boldsymbol{b} \tag{74}$$

where s_0 is the expansion point. The selection of s_0 is discussed in [12]. The PVL algorithm is as follows:

1) Set $\rho_1 = \|\boldsymbol{r}\|_2, \eta_1 = \|\boldsymbol{d}\|_2, \boldsymbol{v}_1 = \boldsymbol{r}/\rho_1$, and $\boldsymbol{w}_1 = \boldsymbol{d}/\eta_1$. Set $\boldsymbol{v}_0 = \boldsymbol{w}_0 = 0$ and $\delta_0 = 1$.
2) For $n = 1, 2, \cdots, q$ do:
   a) Compute $\delta_n = \boldsymbol{w}_n^T\boldsymbol{v}_n$.

b) Set

$$\alpha_n = \frac{\boldsymbol{w}_n^T \boldsymbol{A}\boldsymbol{v}_n}{\delta_n}, \quad \beta_n = \frac{\delta_n}{\delta_{n-1}}\eta_n, \quad \gamma_n = \frac{\delta_n}{\delta_{n-1}}\rho_n.$$

c) Set

$$\boldsymbol{v} = \boldsymbol{A}\boldsymbol{v}_n - \boldsymbol{v}_n\alpha_n - \boldsymbol{v}_{n-1}\beta_n,$$
$$\boldsymbol{w} = \boldsymbol{A}^T\boldsymbol{w}_n - \boldsymbol{w}_n\alpha_n - \boldsymbol{w}_{n-1}\gamma_n$$

d) Set $\rho_{n+1} = \|\boldsymbol{v}\|_2, \eta_{n+1} = \|\boldsymbol{w}\|_2$, and

$$\boldsymbol{v}_{n+1} = \frac{\boldsymbol{v}_n}{\rho_{n+1}}, \quad \boldsymbol{w}_{n+1} = \frac{\boldsymbol{w}_n}{\rho_{n+1}}.$$

3) Construct the tridiagonal matrix,

$$\boldsymbol{T}_q = \begin{bmatrix} \alpha_1 & \beta_2 & 0 & \cdots & 0 \\ \rho_2 & \alpha_2 & \beta_3 & \ddots & \vdots \\ 0 & \rho_3 & \ddots & \ddots & 0 \\ \vdots & \ddots & \ddots & \ddots & \beta_q \\ 0 & \cdots & 0 & \rho_q & \alpha_q \end{bmatrix} \tag{75}$$

4) Compute a decomposition of $\boldsymbol{T}_q$,

$$\boldsymbol{T}_q = \boldsymbol{S}_q \mathrm{diag}(\lambda_1, \lambda_2, \cdots, \lambda_q)\boldsymbol{S}_q^{-1} \tag{76}$$

and set

$$\mu = \boldsymbol{S}_q^T \boldsymbol{e}_1 \quad \text{and} \quad \upsilon = \boldsymbol{S}_q^{-1}\boldsymbol{e}_1 \tag{77}$$

where $e_1 = [1\ 0\ \cdots\ 0]^T$ is the first unit vector.

5) Compute the poles and residues of H_q as

$$p_i = \frac{1}{\lambda_i} \quad \text{and} \quad k_i = -\frac{\mu_i \upsilon_i}{\lambda_i}\boldsymbol{d}^T\boldsymbol{r}. \tag{78}$$

REFERENCES

[1] L. T. Pillage and R. A. Rohrer, "Asymptotic waveform evaluation for timing analysis," *IEEE Trans. Computer-Aided Design*, vol. 9, pp. 352–366, Apr. 1990.

[2] T. K. Tang and M. S. Nakhla, "Analysis of high-speed VLSI interconnects using the asymptotic waveform evaluation technique," *IEEE Trans. Computer-Aided Design*, vol. 11, pp. 341–352, Mar. 1992.

[3] J. Bracken, V. Raghavan, and R. Rohrer, "Interconnect simulation with asymptotic waveform evaluation (AWE)," *IEEE Trans. Circ. Syst. I*, vol. 39, pp. 869–878, Nov. 1992.

[4] S. Lin and E. Kuh, "Transient simulation of lossy interconnects based on the recursive convolution formulation," *IEEE Trans. Circ. Syst. I*, vol. 39, pp. 879–892, Nov. 1992.

[5] C. L. Ratzlaff and L. T. Pillage, "RICE: Rapid interconnect circuit evaluation using AWE," *IEEE Trans. Computer-Aided Design*, vol. 13, pp. 763–776, June 1994.

[6] D. Anastasakis, N. Gopal, S. Kim, and L. Pillage, "Enhancing the stability of asymptotic waveform evaluation for digital interconnect circuit applications," *IEEE Trans. Computer-Aided Design*, vol. 13, pp. 729–735, June 1994.

[7] S.-Y. Kim, N. Gopal, and L. T. Pillage, "Time-domain macromodels for VLSI interconnect analysis," *IEEE Trans. Computer-Aided Design*, vol. 13, pp. 1257–1270, Oct. 1994.

[8] E. Chiprout and M. S. Nakhla, "Analysis of interconnect networks using complex frequency hopping (CFH)," *IEEE Trans. Computer-Aided Design*, vol. 14, pp. 186–200, Feb. 1995.

[9] M. Celik, O. Ocali, M. Tan, and A. Atalar, "Pole-zero computation in microwave circuits using multipoint Padé approximation," *IEEE Trans. Circ. Syst. I*, vol. 42, pp. 6–13, Jan. 1995.

[10] M. Celik, A. Atalar, and M. Tan, "Transient analysis of nonlinear circuits by combining asymptotic waveform evaluation with volterra series," *IEEE Trans. Circ. Syst. I*, vol. 42, Aug. 1995.

[11] M. Celik and A. C. Cangellaris, "Efficient transient simulation of lossy packaging interconnects using moment-matching techniques," *IEEE Trans. Comp., Packag., Manufact. Technol., B*, vol. 19, pp. 64–73, Feb. 1996.

[12] P. Feldmann and R. W. Freund, "Efficient linear lircuit analysis by Padé approximation via the Lanczos process," *IEEE Trans. Computer-Aided Design*, vol. CAD-14, pp. 639–649, May 1995.

[13] C. Canuto, M. Y. Hussaini, A. Quarteroni, and T. A. Zang, *Spectral Methods in Fluid Dynamics*. Springer Series in Computational Physics, Berlin, Heidelberg: Springer-Verlag, 1987.

[14] O. A. Palusinski and A. Lee, "Analysis of transients in nonuniform and uniform multiconductor transmission lines," *IEEE Trans. Microwave Theory Tech.*, vol. 37, pp. 127–138, Jan. 1989.

[15] C. W. Ho, A. E. Ruehli, and P. A. Brennan, "The modified nodal approach to network analysis," *IEEE Trans. Circuit Theory*, vol. CAS-22, pp. 504–509, June 1975.

[16] P. Feldmann and R. W. Freund, "Reduced-order modeling of large linear subcircuits via a block Lanczos algorithm," in *Proc. Design Automation Conf.*, June 1995.

[17] T. L. Quarles, "The SPICE3 implementation guide," Tech. Rep. Memo ERL-M89/44, Univ. of California, Berkeley, Apr. 1989.

[18] L. P. Vakanas, A. C. Cangellaris, and J. L. Prince, "Frequency-dependent [L] and [R] matrices for lossy microstrip lines," *Trans. Soc. Computer Sim.*, vol. 8, pp. 295–318, Dec. 1991.

[19] The Math Works, Inc., Natick, MA, *MATLAB User's Guide*, 1992.

Mustafa Celik was born in Konya, Turkey, in 1966. He received the B.S. degree from Middle East Technical University, Ankara, Turkey in 1988, and the M.S. and Ph.D. degrees from Bilkent University, Ankara, Turkey, in 1991 and 1994, respectively, all in electrical engineering.

He is a Research Associate in the Department of Electrical and Computer Engineering at Carnegie Mellon University, Pittsburgh, PA. From 1994 to 1996 he worked in the Department of Electrical and Computer Engineering at the University of Arizona. His research interests include circuit, interconnect, and mixed-signal simulation.

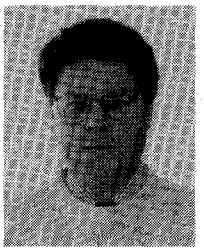

Andreas C. Cangellaris (M'86) received the Diploma in electrical engineering from the Aristotle University, Thessaloniki, Greece, and the M.S. and Ph.D. degrees in electrical engineering from the University of California, Berkeley, in 1983 and 1985, respectively.

During 1985–1987, he was with the Electronics Department of General Motors Research Laboratories in Warren, MI. In 1987 he joined the Department of Electrical and Computer Engineering at the University of Arizona, where he is now an Associate Professor. His research interests are in computational electromagnetics, microwave engineering, and algorithm development for high-speed digital circuit analysis. His research in computational electromagnetics has emphasized differential equation-based techniques, both in the frequency and time domain. He has published over 50 journal papers in those areas.

Dr. Cangellaris is an Associate Member of the International Union of Radio Science (URSI). In 1993, he received the International Union of Radio Science (URSI) Young Scientist Award. He is an active member of the following IEEE Societies: Antennas and Propagation; Microwave Theory and Techniques; and Components, Packaging and Manufacturing Technology.